The Structure of the Photon and the Proton

Allen C. Caldwell
Physics Department, Columbia University
New York City, NY 10027, USA
E-mail: caldwell@ nevis.columbia.edu

ABSTRACT

The study of the structure of the photon and proton reveals information on the strong and electromagnetic force, and allows to discriminate between different theoretical models. Recent experimental results are reviewed and compared to the predictions and parametrizations for the photon and proton structure.

1. Introduction

The concept of photon structure seems at first paradoxical. Real photons are massless, and have no permanent structure. Photon structure has historically been probed in photon-photon scattering, but classically photons do not interact with each other. Quantum mechanically, the photon can fluctuate into charged particle-antiparticle pairs such as electron-positron or quark-antiquark. This fluctuation is only present for a short time, but this allows the photon to have a structure. When we speak of photon structure we are studying quantum fluctuations of the photon state, and the photon-photon interaction can be viewed as the scattering of one photon on the fluctuation of the other photon. The measurement of the structure allows the study of both QED (quantum electrodynamics) and QCD (quantum chromodynamics). The latter can be studied in the case when the photon fluctuates into a quark-antiquark pair, which can further produce gluons and more quarks.

The proton has a "real" structure consisting of quarks and gluons as well as a "virtual" structure similar to that of the photon. Measurements of the proton structure are therefore well suited to the study of QCD.

1.1. Probes for Measuring Photon and Proton Structure

The photon structure has historically been measured in e^+e^- experiments, where a photon radiated from the positron interacts with a photon radiated from the electron. It is also possible to probe the photon structure using quarks and gluons as probes (e.g., in ep collisions). In studying proton structure, photons, weak bosons (Z, W), quarks and gluons have all been used to probe the structure. A key element in our description of these interactions is the concept of factorization. The cross section for the interaction is written as the convolution of a flux for the probe (Γ_{probe}), a density of partons in the struck object (f_{parton}), and a scattering cross section for the probe

and parton ($\hat{\sigma}$):

$$\sigma \sim \Gamma_{probe} \otimes f_{parton} \otimes \hat{\sigma} \ . \tag{1}$$

The scattering cross sections for different combinations of probes and partons can be calculated in the standard model (electroweak theory+QCD) in some approximation provided a sufficiently high energy scale is present. The flux of the probe is usually well known, and the parton densities are assumed to be universal. This factorization has been proven for some specific cases [1], but remains in the general case an assumption. Studying the photon and proton structure with different probes allows a test of this assumption.

1.2. Parton Densities and Scales

The transverse dimensions at which the parton densities are probed depend inversely on the (transverse) energy scale at which the scattering takes place. For instance, the transverse distance probed by a photon of (negative) mass squared $Q^2 = 4$ GeV^2 is $\sim 10^{-14}$ cm. More structure is revealed as the energy scale is increased. This implies that the number of partons with smaller momentum fraction (x) increases with increasing energy scale, while the number at higher x correspondingly decreases. The precise nature of the evolution of the parton densities in (x, Q^2) is a fundamental issue addressed by structure function measurements. QCD predicts the evolution as a function of Q^2, and these predictions can be compared to data.

In general, calculations of scattering cross sections in QCD can only be performed if a "hard" scale is present. Calculations are performed in perturbation theory, and only converge if (among other constraints) α_S, the coupling constant for the strong force, is relatively small. The value of α_S decreases with increasing scale, and above some scale is small enough so that perturbation theory is thought to be reliable. This hard scale can be Q, transverse energy, or mass. The value of the scale above which perturbative QCD (pQCD) calculations are valid is not known, but this value was expected to be a few GeV. Recent data from E665 and HERA indicate that pQCD calculations are still valid at scales as low as 1 GeV. The validity of pQCD calculations at small scale values is one of the more interesting topics in the study of QCD.

Reliable knowledge of parton densities, particularly at small–x, are very important for cross section calculations at current and future accelerators. There has been considerable experimental progress in this area in recent years. Some of these new results are summarized below.

2. Photon Structure in e^+e^- Experiments

The structure of photons has traditionally been studied in e^+e^- experiments, where a photon from the positron interacts with a photon from the electron. This scattering process is shown in Fig. 1. In this figure, the incoming and outgoing lepton

four-vectors are given in parentheses. We can construct the invariants:

$$\begin{aligned} Q^2 &= -q^2 = -(k-k')^2 = 4E_0E_1'\sin^2(\theta_1'/2) \\ P^2 &= -p^2 = -(l-l')^2 = 4E_0E_2'\sin^2(\theta_2'/2) \\ W^2 &= (p+q)^2 \\ x &= \frac{Q^2}{2p\cdot q} = \frac{Q^2}{Q^2+W^2} \\ y &= \frac{p\cdot q}{p\cdot k} = 1-(E_1'/E_0)\cos^2(\theta_1'/2) \end{aligned}$$

where the negative of the photon mass squared (virtuality) are given by Q^2 and P^2, and the invariant mass of the two photon system is W. The variable x is analogous to the usual x–Bjorken in deep inelastic scattering; i.e., in the infinite momentum frame it is the fraction of the target momentum carried by the struck quark. In the target photon rest frame, the variable y represents the fractional energy carried by the probing photon. The electron beam energy is denoted by E_0, while the scattered electron energies and angles are given by E', θ'.

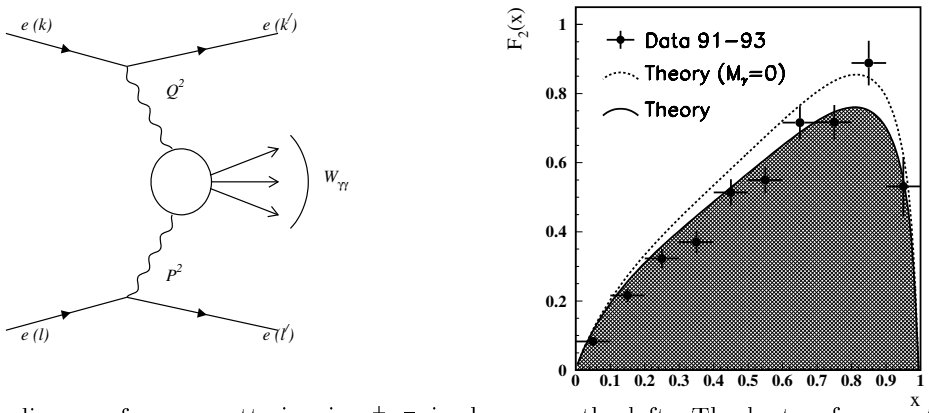

Fig. 1. The diagram for $\gamma\gamma$ scattering in e^+e^- is shown on the left. The lepton four vectors are given in parentheses. Preliminary results on $F_2^{\gamma,QED}$ from L3 are shown in the right plot. The QED prediction including finite P^2 is shown as the shaded region.

The scattered electrons can either be untagged, singly tagged, or doubly tagged. When a tag is present, Q^2 is generally assigned to the photon with the larger virtuality. The higher virtuality photon is then pictured as probing the structure of the lower virtuality photon. In the case of singly or doubly tagged photons, and assuming an average over azimuthal angles, we can then write the differential cross section as:

$$\frac{d^2\sigma}{dxdQ^2} = \frac{2\pi\alpha^2}{xQ^4}\left[(1+(1-y)^2)F_2^\gamma(x,Q^2) - y^2F_L^\gamma(x,Q^2)\right]N_\gamma(z,\theta'_{2,max})zdz \qquad (2)$$

where the function N represents the flux of target photons. Note that F_2^γ can be split into $F_2^{\gamma,QED}$, where the photon fluctuates into a lepton pair, and $F_2^{\gamma,QCD}$, where

the photon fluctuates into a quark-antiquark pair or a more complicated hadronic configuration. Experimentally, it is usually the case that y is small (< 0.1) such that the F_L term is neglected.

2.1. Electromagnetic Structure of the Photon

$F_2^{\gamma,QED}$ is calculable in QED and is therefore well known. Recent measurements of this quantity have been performed by DELPHI [2] and L3 [3] looking at the process $e^+e^- \rightarrow e^+e^-\mu^+\mu^-$. The comparison of the L3 results with expectations from QED calculations are shown in Fig. 1. They are found to be in good agreement once the ≈ 10 % correction is applied for the non-zero value of P^2. L3 has additionally looked at angular distributions to gain access to other structure functions besides F_2.

2.2. Hadronic Structure of the Photon

Historically, $\gamma\gamma$ scattering was proposed as an ideal laboratory for studying QCD. In leading order (LO) [4],

$$\begin{aligned} F_2^{\gamma,QCD} &= \sum_q e_q^2 x q(x,Q^2) \\ &\sim \sum_q e_q^4 \left[a(x) + b(x) \ln \frac{Q^2}{\Lambda^2} \right] \end{aligned}$$

where a, b are calculable functions, e_q is the quark charge, and $q(x,Q^2)$ represents the quark density. In LO, therefore, a measurement of F_2 would yield a measurement of Λ_{QCD}, the scale of the strong interaction. However, NLO order calculations have shown that this simple relationship breaks down, and there are problems in the calculation at both large and small x (for a review of the history, see [5,6]). As with the proton, it has turned out that it is necessary to parametrize the parton density. There is still theoretical hope [7] that the structure of the virtual photon is calculable. This will no longer provide a direct measurement of Λ_{QCD} since Λ^2 will be replaced by the scale P^2. Nevertheless, measurements of the photon structure are very interesting since the Q^2 dependence of the structure function is predicted by QCD.

Recent measurements on the Q^2 evolution of $F_2^{\gamma,QCD}$ by OPAL [8], DELPHI [2] and AMY [9] are shown in Fig. 2 along with previous measurements. The OPAL points are at average Q^2 values of $101, 202$ GeV^2, the DELPHI point is given at 12 GeV^2, and the AMY values are at $73, 390$ GeV^2. The curves in the figure show the expectations from a QCD based model [8,10]. As can be seen, the results are in good agreement with the expected $\ln(Q^2)$ behavior over two orders in magnitude in Q^2.

While the Q^2 dependence is predicted in QCD, the x-dependence is much less well constrained. This has led to a host of parametrizations which give a wide range of values in the unmeasured regions, particularly at small–x. These parametrizations

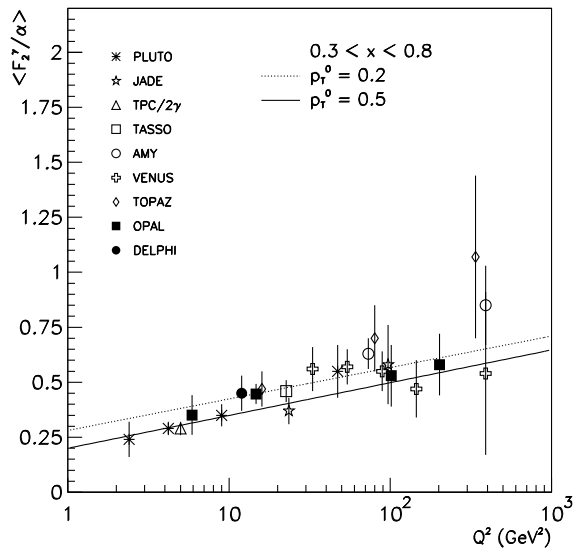

Fig. 2. A summary of recent results on $F_2^{\gamma,QCD}$ as a function of Q^2 in the range $0.3 < x < 0.8$. Note that the OPAL and DELPHI results shown here are preliminary. The curves are from a QCD model [8,10].

are based on different assumptions, and determining which are most successful may yield insight into the dynamical mechanism responsible for the parton distributions. Recent results are available from DELPHI [2], OPAL [8] and TOPAZ [11] on $F_2^{\gamma,QCD}$ in the range $x < 0.3$, where current parton density parametrizations start to disagree strongly in their predictions. The existing data are not in very good agreement with each other, but the tendency is to favor parton densities which are not steeply rising at small–x, such as GRV [12] or GS [13], rather than steeply rising parton densities such as LAC1 [14] or DO [15].

LEPII is currently being brought into operation. With this accelerator, there will be an increased flux of real and virtual photons, improved detectors for $\gamma\gamma$ physics, and lower backgrounds. The future of these kinds of measurements therefore looks bright, and we may hope to see more stringent tests of QCD performed with these data.

3. Photon Structure at HERA

3.1. Resolved and Direct Photons

The study of photon structure at the ep collider HERA is less direct than at e^+e^- machines. Two generic classes of events can be defined (in LO), as shown in Fig. 3.

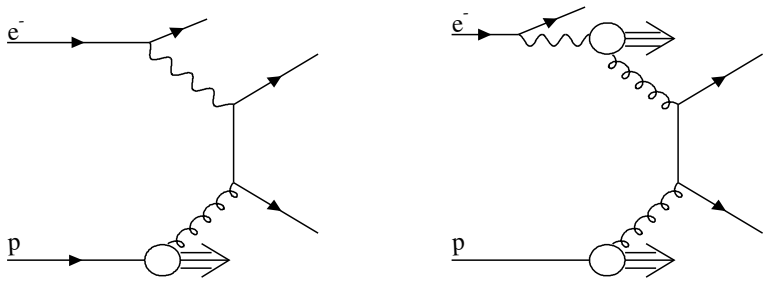

Fig. 3. a) Direct photoproduction event. b) Resolved photoproduction event.

The two classes are denoted "direct", where the photon couples to a quark producing a jet, and "resolved", where a parton from the photon is involved in the hard interaction. In the direct case, the full photon 4-momentum is present in the interaction, while in the resolved case, only a fraction of the photon 4-momentum is transfered to the jet system. The hard scale at which the probe measures the photon is provided by the jet transverse energy, E_T. Although the structure of the photon is not measured directly, this type of scattering is sensitive to the parton distributions in the photon (and the proton).

The fractional momentum of the photon which enters into the hard interaction can be calculated (in LO) from the outgoing partons as can the fractional momentum of the proton momentum, as follows:

$$\begin{aligned} x_\gamma^{LO} &= \frac{\sum_{partons} E_T e^{-\eta}}{2E_\gamma} \\ x_p^{LO} &= \frac{\sum_{partons} E_T e^{\eta}}{2E_p} \end{aligned}$$

Note that in the HERA convention, $\eta > 0$ is in the direction of the proton beam, with the pseudorapidity $\eta = -\ln\tan(\theta/2)$. Experimentally, the parton momenta are replaced by the corresponding jet quantities:

$$\begin{aligned} x_\gamma^{Obs} &= \frac{\sum_{jets} E_T e^{-\eta}}{2E_\gamma} \\ x_p^{Obs} &= \frac{\sum_{jets} E_T e^{\eta}}{2E_p} \,. \end{aligned}$$

Given these definitions, we expect $x_\gamma^{Obs} \approx 1$ for direct processes, and $x_\gamma^{Obs} < 1$ for resolved processes. The values will depend on the experimental reconstruction scheme for the jets and for E_γ. A rather clean separation of these two classes of events can be performed when two jets are found in the event. An example is shown from the

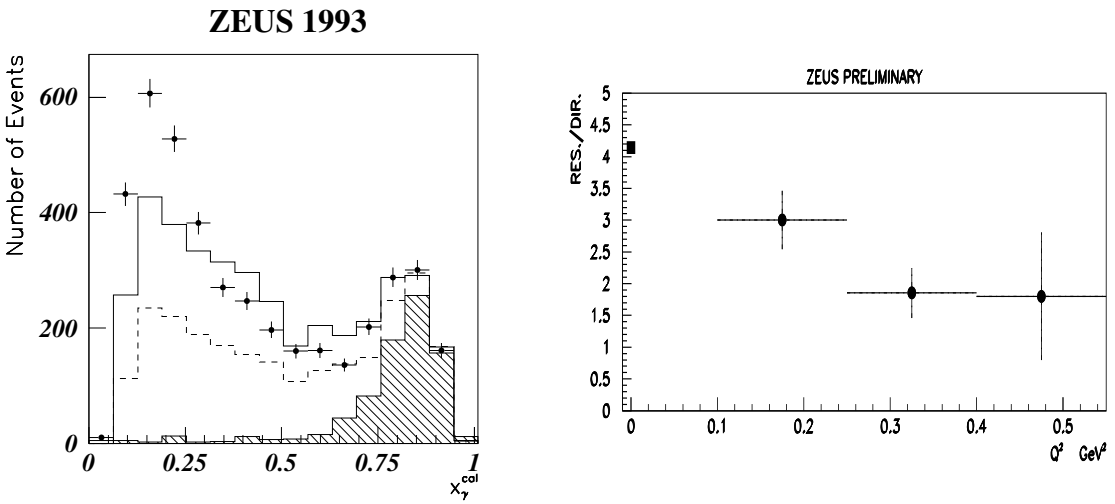

Fig. 4. The distribution in x_γ^{Obs} from ZEUS for a selected sample of two jet events is shown in the left hand plot. The preliminary ZEUS results on the ratio of resolved to direct events as a function of the virtuality of the photon is shown on the right.

ZEUS experiment in Fig. 4. The ZEUS collaboration defines the direct sample with a cut $x_\gamma^{Obs} > 0.75$.

Figure 4 was made for untagged photoproduction events ($Q^2 < 4$ GeV^2, $Q^2_{Avg} \approx 10^{-3} - 10^{-4}$ GeV^2), which is dominated by almost real photons. It is expected that the fraction of resolved photons will decrease as the virtuality of the photon decreases [16]. This has been tested by ZEUS using tagged events in the virtuality range $0.1 \rightarrow 0.55$ GeV^2. The preliminary result on the ratio of resolved to direct events is shown in Fig. 4 as a function of Q^2. The data are in qualitative agreement with the expectations.

3.2. Jet Rates and QCD Tests

The hard scale provided by jets in photoproduction allows comparisons with QCD calculations. H1 [17] and ZEUS [18] have published inclusive jet differential cross sections in photoproduction. In NLO, three different scales must be distinguished—the renormalization scale (μ), the factorization scale for the parton density in the proton (μ_p), and the factorization scale for the parton density in the photon (μ_γ). The separation of direct and resolved events in NLO depends on μ_γ. The ZEUS measurement of $d\sigma/d\eta^{jet}$ is shown in Fig. 5 for three different minimum jet E_T values (8, 11, 17 GeV), compared to NLO calculations from Aurenche et al. [19] (ACFGP) and Klasen, Kramer and Salesch [20] (KKS). The theoretical predictions are for the scale choices $\mu = \mu_p = \mu_\gamma = E_T$. Large discrepancies are found, particularly for $\eta^{jet} < 0$, where calculations were originally expected to be most accurate. From kinematic considerations, it is clear that the region $\eta^{jet} < 0$ is populated by high x_γ events.

This would imply a preponderence of direct photoproduction events, which are believed to be well understood. However, recent calculations [21] for dijet cross sections in photoproduction have been compared to ZEUS data [22] and indicate that there is a large uncertainty in the contribution of resolved photoproduction events for these large values of x_γ. Note that there are few measurements of $F_2^{\gamma,QCD}$ at values of $x_\gamma \geq 0.8$.

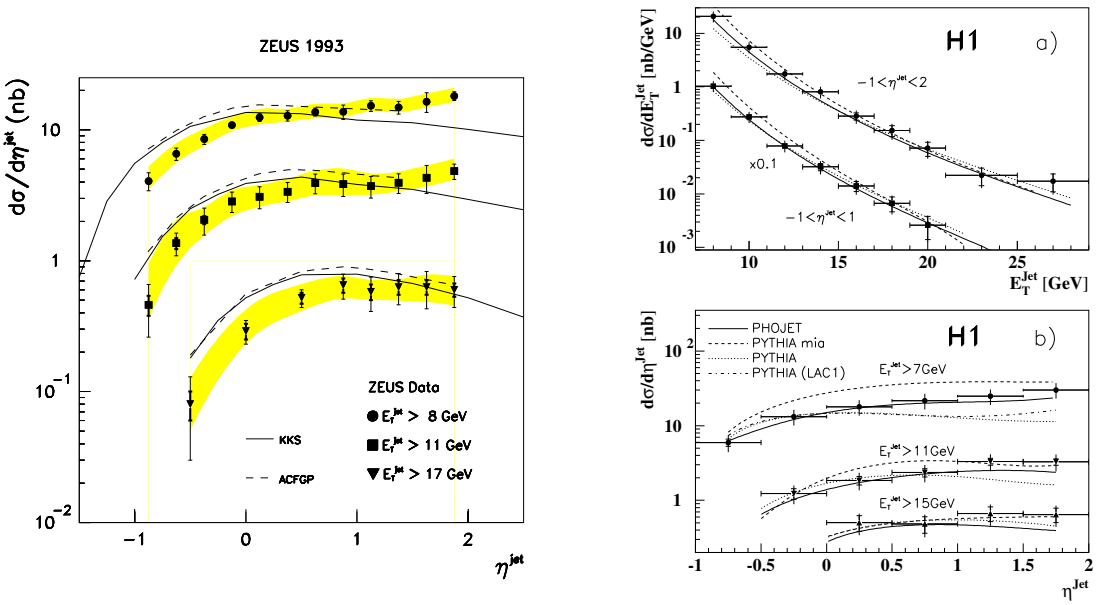

Fig. 5. The ZEUS inclusive jet differential cross section vs. η^{jet} for three different minimum jet E_T values are compared to NLO calculations in the left hand plot. The H1 data on the E_T distribution are compared to a LO MC with and without multiple interactions (see text) in the upper right plot. The lower right hand plot shows the jet differential cross section verus η^{jet}.

3.3. Energy Flows and Multiple Interactions

The disagreement between data and theoretical calculations for positive η^{jet} is also seen in the E_T distributions. The H1 collaboration has studied this energy excess in the forward direction [23] and has found that it could in large part be explained by multiple interactions between partons from the photon and those from the proton [24]. Results from H1 on the inclusive jet cross section are shown in Fig. 5 for different E_T thresholds. The data are compared to PHOJET [25] (LO with multiple interactions) and PYTHIA [26] (LO plus parton showers without multiple interactions) Monte Carlo (MC) calculations. The agreement is clearly better for the PHOJET MC. H1 concludes that multiple interactions are likely necessary to explain the energy flows.

3.4. The Gluon Density in the Photon

H1 has modelled photoproduced dijet events with PYTHIA 5.6 including multiple

interactions. The photon and proton parton densities were taken from GRV(LO) [27,28] and the parameters for the multiple interactions from fits to $p\overline{p}$ data [29]. This MC was found to give improved agreement with the data. The MC was used to unfold observed distributions to extract distributions at the partonic level, and the gluon density in the photon was extracted (in LO) [30] by subtracting the contribution from direct photon events and the resolved contribution from quarks. The results are shown in Fig. 6 at the scale $< p_t >^2 = 75$ GeV^2. The data (as with $F_2^{\gamma,QCD}$ discussed in the previous section) are more compatible with parton distributions which do not have a steep rise at small–x.

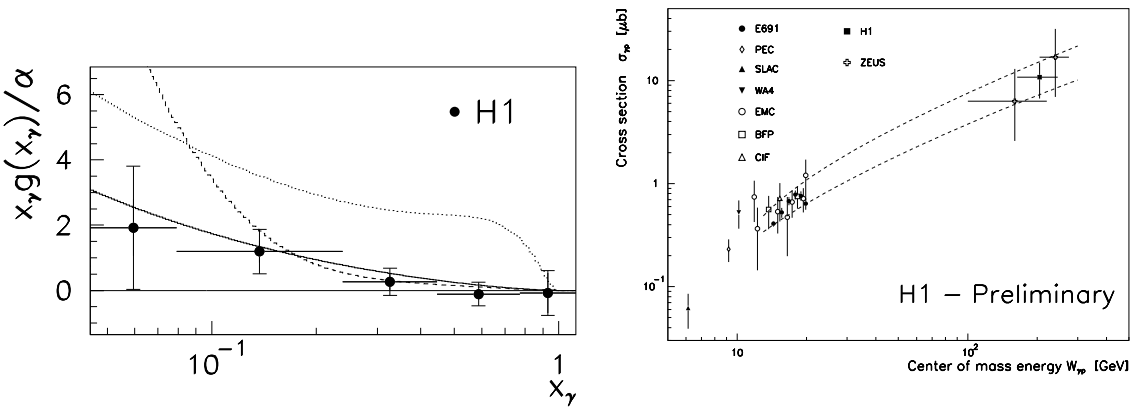

Fig. 6. The gluon momentum density in the photon in LO from the H1 collaboration is shown on the left. The data are compared to parametrizations from GRV [27] (full line), LAC1 [14] (dashed line), and LAC3 [14] (dotted line). The total $c\overline{c}$ photoproduction as a function of W from H1 and ZEUS, extracted from the measured D^* cross sections is shown on the right. The dashed line represents the QCD prediction using the MRS-G parton densities for the proton and GRV-G(HO) parton densities for the photon. The effect of changing the renormalization scale in the range $0.5 < \mu/m_c < 2.0$ is shown by the variation of the prediction.

Multiple interactions should only be present in resolved photon processes. The ZEUS collaboration has studied the forward energy flow separately for resolved and direct events [31] and indeed finds that the excess is principally in the resolved events. Multiple interactions are possibly the explanation for the forward energy flow excess seen at HERA. This would however complicate an already complicated situation. Multiple interactions, where two partons in the photon interact with the proton, would violate the simple form of factorization presented in Eq. 1. Also, the level of multiple interactions depends strongly on the parton density in the photon, so that a good MC description of photoproduction events will require the tuning of many parameters.

3.5. Heavy Quark Production

The production of charm quarks in photoproduction has been studied as a potentially interesting method for probing the gluon content of the proton via the photon–gluon fusion diagram. The hard scale would in this case be provided by the charm

mass. The cross section for charm production has been determined by the ZEUS [32] and H1 [33] experiments using the measured D^* cross section, and the results are shown in Fig. 6. The results are compared to QCD calculations [34] using the MRS-G [35] parton densities for the proton and the GRV-G(HO) parton densities for the photon [12], with different choices for the renormalization and factorization scales. The calculations are seen to be in broad agreement with the data. However, this process could also be interesting as a probe of the charm quark density in the photon. An interesting contribution to this conference by Drees and Godbole [36] suggests that in addition to the direct and resolved production of $c\overline{c}$, there is also the possibility that the charm content of the photon is excited (here a charm quark from the photon takes part in the interaction). In this case, only one of the jets would contain charm, with the balancing flavor being in the photon remnant. Search strategies to look for this are proposed in the preprint.

3.6. Conclusions and Outlook for Photon Structure Studies at HERA

It is seen that resolved and direct contributions can be rather clearly separated at HERA, and that the relative contribution from the direct events increases with increasing photon virtuality. The ability to make this separation would indicate that the photon structure can be studied. However, comparisons with LO and NLO QCD calculations on jet rates show that much remains to be understood, both in the direct photoproduction as well as in the resolved photoproduction. There are indications that multiple interactions are present in resolved photoproduction, which greatly complicates the analysis of the data. Despite this fact, a first measurement of the gluon density of the photon has been made (in LO) using a MC model with multiple interactions to unfold the data. Clearly much more work needs to go into a detailed understanding of the final state.

The intense experimental activity is matched by intense theoretical activity. NLO calculations are becoming available for more and more processes, such as heavy quark production. It is via comparisons to these more accurate calculations that progress in our understanding can be expected.

4. The Structure of the Proton

The structure of the proton has been studied in great detail in fixed target experiments using electron, muon and neutrino beam, in $p\overline{p}$ colliders and at the ep collider HERA. These experiments are sensitive to different regions in (x, Q^2), and the different probes allow a test of factorization.

The diagram describing deep inelastic scattering (DIS) by one photon exchange in electron (or muon)–hadron scattering is shown in Fig. 7. The variables used to

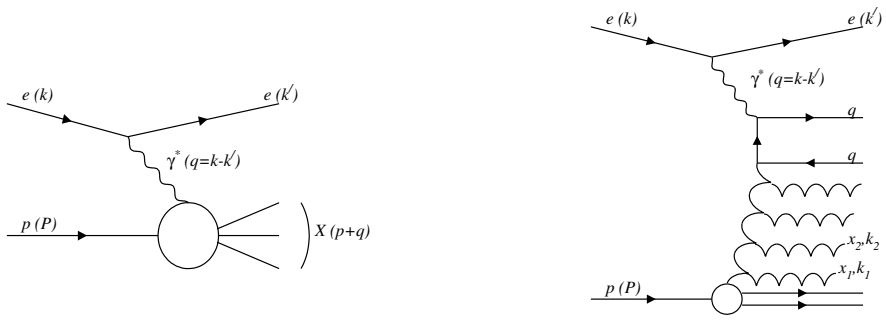

Fig. 7. The basic diagram for one photon exchange in ep scattering is shown on the left. The four–vectors are shown in parentheses. An example diagram for a small–x event is shown on the right. Here the struck quark comes from a long chain of branching processes.

describe the scattering are:

$$\begin{aligned} Q^2 &= -(k-k')^2 \\ x &= \frac{Q^2}{2P\cdot q} \\ y &= \frac{2P\cdot q}{2P\cdot k} \end{aligned}$$

where the four–vectors are defined in the figure. The scaling variables x and y have intuitive meaning in special reference frames — x represents the fractional momentum of the proton carried by the struck quark in the frame where the proton has infinite momentum, while y is the fractional energy of the electron carried by the photon in the proton rest frame. The transverse distance scale at which the proton structure is probed is inversely proportional to Q. Note that only two of the three variables are independent, as they are related to the total center of mass energy $s = (P+k)^2$ by $Q^2 = sxy$. Another variable frequently used in the description of high energy scattering is the invariant mass of the system X, labelled W, defined by $W^2 = (P+q)^2 = m_P^2 + Q^2(1-x)/x$. At small values of x, $W \approx Q^2/x = sy$. The differential cross section described by Fig. 7 for $Q^2 << M_{W,Z}^2$ is given by:

$$\frac{d^2\sigma}{dxdQ^2} = \frac{2\pi\alpha^2}{xQ^4}\left[(1+(1-y)^2)F_2(x,Q^2) - y^2F_L(x,Q^2)\right] . \qquad (3)$$

In the quark-parton model

$$\begin{aligned} F_2 &= \sum_q e_q^2 xq(x) \\ F_L &= 0. \end{aligned}$$

In QCD, F_2 aquires a Q^2 dependence, and F_L is no longer zero beyond LO. The structure function F_2 still basically depends on the quark densities (although the definition is renormalization scheme dependent), but the Q^2 evolution of F_2 depends

on both the quark $q(x,Q^2)$ and gluon $g(x,Q^2)$ densities in the proton. The virtual photon depicted in Fig. 7 must couple to a quark. At small values of x, this quark is possibly the result of a long chain of branching processes, such as that shown in Fig. 7. The x distribution of quarks and gluons depends on the scale at which they are probed. The evolution of this distribution with the scale is to date very well described by the DGLAP [37] evolution equations, which are perturbative calculations in powers of $\alpha_S \ln Q^2$ (in leading log approximation). There is currently considerable interest in determining whether this evolution formalism is still adequate at small–x, or whether the BFKL formalism [38], which is a perturbative calculation in powers of $\alpha_S \ln 1/x$ is perhaps more appropriate. A detailed review of these issues can be found in the report of Jochen Bartels in these proceedings. These evolution equations are linear, in the sense that one parton will always split into two partons. However, at high enough parton densities, it is also expected that parton recombination could occur [39]. In this case, the evolution equation would depend on the square of the parton densities. So far, no sign has been seen of parton recombination effects.

4.1. Parton Density Parametrizations

The photoproduction and hadron scattering cross sections are well described by Regge theory inspired phenomenology. Donnachie and Landshoff [40] have used this cross section behavior to parametrize F_2 for Q^2 values up to ≈ 10 GeV^2. In their model, $F_2 \sim x^{-n}$ at small x, where $n = 0.08$. In the following, their parametrizations will be labelled DoLa (or sometimes DL). Their parametrization was determined before the advent of HERA data (and recent E665 data), and is therefore a prediction for the small–x behavior of the structure functions. Another prediction comes from Glück, Reya and Vogt (GRV) [28]. They input "valence-like" parton distributions at a small value of Q^2, $Q_0^2 < 0.4$ GeV^2, and use the DGLAP evolution to predict the parton distributions at higher values of Q^2. These two very different sets of parton densities are compared in Fig. 8. They show strikingly different behavior at small–x in the Q^2 interval from $0.3 \rightarrow 0.9$ GeV^2. Above these values of Q^2, the GRV values of F_2 at small–x are considerably larger than those of DoLa. The GRV parton distributions have been found to give good agreement with previous HERA data [28]. At some value of Q^2 we expect a transition from the perturbative QCD description to a Regge type description. Recent data from E665 and the HERA experiments yield more information on this question, as will be discussed in the following sections.

In the approach of Martin, Roberts and Stirling (MRS) [41] and the CTEQ collaboration [42], the parton densities are parametrized at a scale $Q_0^2 \approx 2.5 - 4.0$ GeV^2 and evolved with the NLO DGLAP formalism. These parameters are derived from best fits to a large sample of data from many different experiments. They are routinely updated as new data become available, and represent our best estimates for

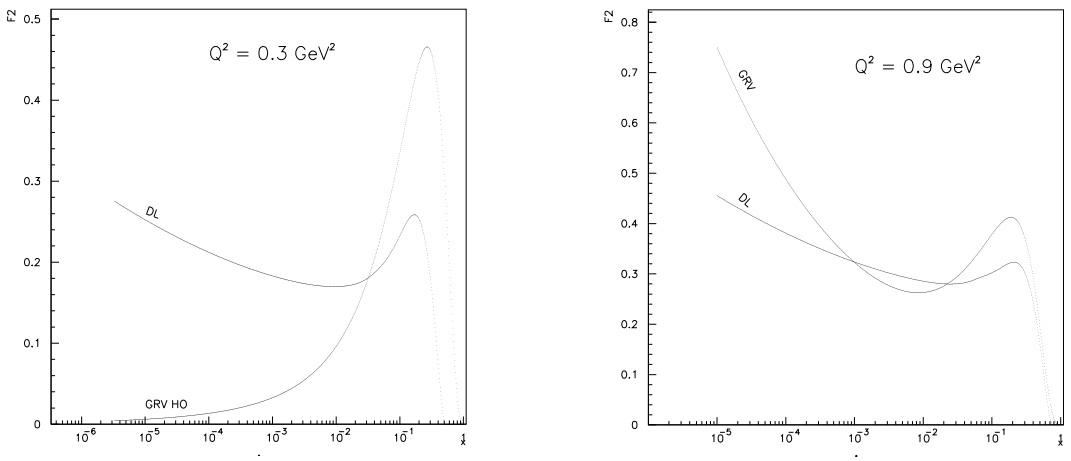

Fig. 8. Comparison of F_2^p predictions versus x from DoLa and GRV at Q^2 values of 0.3 GeV^2 and 0.9 GeV^2.

the parton distributions.

5. Recent Results from Fixed Target Experiments

5.1. Recent NMC Results

NMC has recently analyzed data sets at energies (120, 200 GeV) [43] intermediate to those already published (90, 280 GeV) [44]. These new data sets allow the measurement of F_2 in kinematic regions intermediate to those previously reached by NMC. They also overlap the previous kinematic regions, providing a valuable check on the systematic errors in the measurement. The different y values at the same (x, Q^2) in the overlapping regions should allow NMC to extract a measurement of F_L (see Eq. 3).

The combined data of NMC, SLAC [45] and BCDMS [46] for F_2^d are shown in Fig. 9. These data span over two orders of magnitude in x and Q^2. They are precise and in very good agreement with each other. The expectations of decreasing (increasing) F_2 with Q^2 for large–x (small–x) is beautifully demonstrated by these data. NMC has parametrized these data with a 15 parameter function [47], and fitted this parametrization to the data sets. The relative normalizations of the data sets were left free in the fit, and were found to range from $-2.5 \rightarrow +1.5$ % from the nominal values. Correlated errors have been taken into account in the fit. The resulting parametrization is shown as the solid line in the figure, while the uncertainty (which ranges from $2-4$ % at small–x to 1.5 % at large–x) is shown by the dashed line.

The NMC collaboration has also compared their data on F_2^d to recent measure-

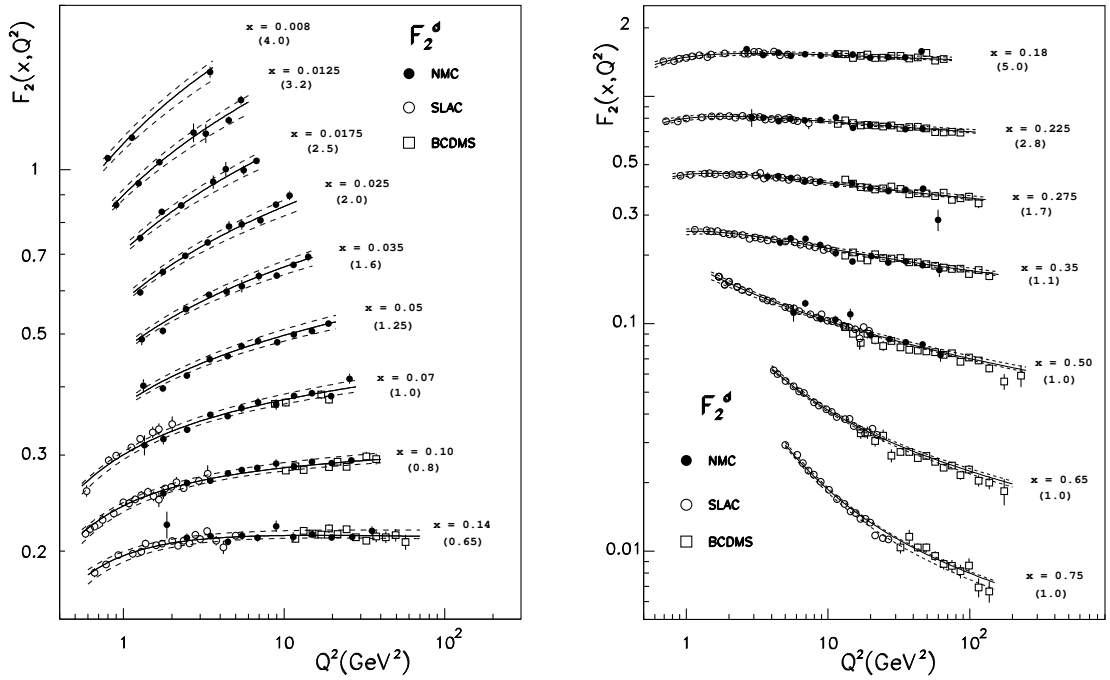

Fig. 9. Summary of NMC, SLAC and BCDMS data for F_2^d. The NMC data are shown as solid circles, the SLAC data as open circles, and the BCDMS data as squares. The solid line is a parametrization determined by the NMC collaboration. The dashed line represents the uncertainty in the parametrization.

ments from the E665 collaboration [48], and their data on F_2^p to HERA data [49,50]. In both cases, good agreement is found. There remains however a difference between the NMC and CCFR [52] structure function measurements at small–x. The CCFR data are for a neutrino beam on an iron target. They have been corrected for the differences between muon and neutrino beams, and for nuclear effects. A discrepancy of > 10 % between the results is found over a wide range in Q^2. Many possible sources for this disagreement have been studied (radiative corrections, large strange sea, nuclear effects), but none explain the difference [52]. This discrepancy will most likely have to be resolved by future experiments.

5.2. Recent E665 Data

The recent E665 data [48] at small–x and small–Q^2 are compared to the DoLa and GRV predictions in Fig. 10. There is good agreement between the data and these predictions down to $x = 0.002$ for the Q^2 values measured. Below this x value, and below $Q^2 = 0.5$ GeV^2, the data favor DoLa. The agreement of GRV with the data down to such low Q^2 comes as a major surprise to most experts working in this field.

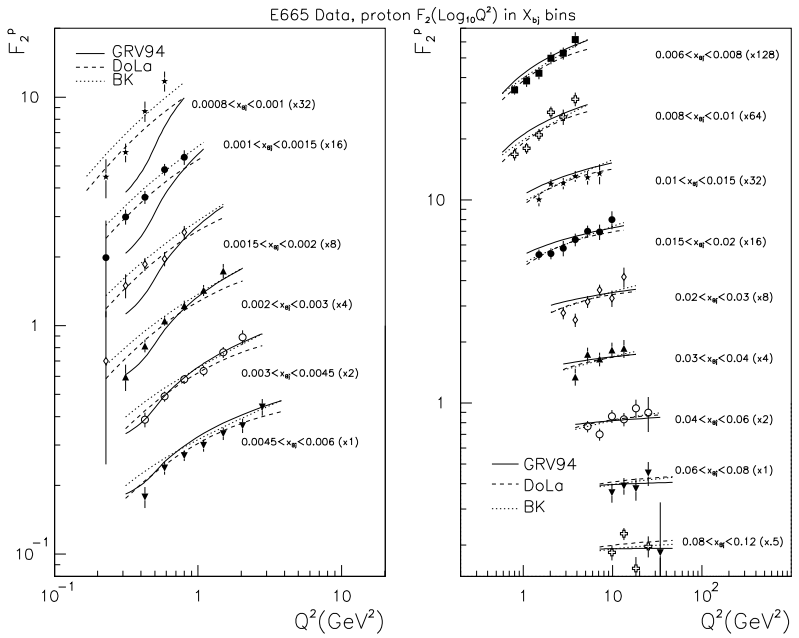

Fig. 10. Comparison of recent E665 data for F_2^p to predictions from DoLa, GRV and BK [51].

5.3. GLS Sum Rule and α_S from CCFR

An interesting analysis, using measured structure functions, of the Gross–Llewellyn Smith [53] sum rule by the CCFR collaboration [54] has provided a new measurement of α_S. The GLS sum rule predicts in LO that the integral of the non-singlet structure function F_3 should give precisely the number of valence quarks in the proton. Higher order QCD corrections changes the prediction [55]:

$$\int_0^1 F_3(x,Q^2)dx = 3\left(1-\frac{\alpha_S}{\pi}-a(n_f)(\frac{\alpha_S}{\pi})^2-b(n_f)(\frac{\alpha_S}{\pi})^3\right)-HT \qquad (4)$$

where the coefficients a, b are calculated and depend on the number of flavors, n_f, and HT represents higher twist contributions [56]. CCFR has performed a combined analysis of different neutrino scattering data [57] and have used the SLAC measurements [45] of F_2 to constrain xF_3 for $x > 0.5$. The resulting xF_3 values are shown in Fig. 11. The integral of xF_3 is then plotted as a function of Q^2 as shown, and a fit for $\Lambda_{\overline{MS}}$ is performed using the Q^2 dependence [58] of the measured α_S. The resulting measurement of α_S is

$$\alpha_S(M_Z) = 0.108^{+0.003}_{-0.005}(\text{stat}) \pm 0.004(\text{syst})^{+0.004}_{-0.006}(\text{HT}). \qquad (5)$$

6. Proton Structure Function Measurements at HERA

The HERA accelerator started producing data in 1992, and the experiments ZEUS

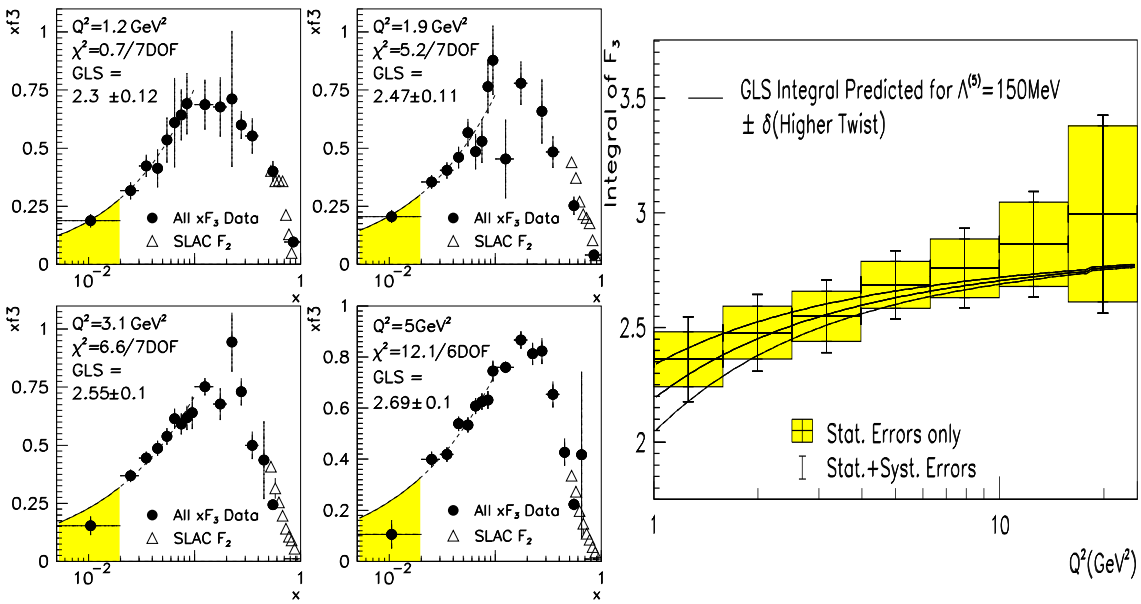

Fig. 11. Combined data on xF_3 as compiled by the CCFR collaboration. The integral of F_3 as a function of Q^2 is shown on the right along with the fit to the form given in eq. 4.

and H1 have now each published two sets of proton structure function measurements [49,50,59,60]. The first measurements showed the now well known rise of F_2^p with decreasing x at small–x. These results were confirmed with the 1993 data. In addition, F_2 was found to depend essentially only on W in the kinematic range measured, and double asymptotic scaling [61] was determined to hold. First extractions of the gluon density in the proton were also performed [62,63]. In this report, we will concentrate on the preliminary results from the 1994 data run. The main improvement to date from this data set has been the extension of the measured kinematic range down to $Q^2 \geq 1.5$ GeV^2.

6.1. Recent low–Q^2 Measurements from HERA

We can write Q^2 in terms of the scattered electron variables as follows:

$$Q^2 = 4E_e E'_e \sin^2 \frac{\theta_e}{2} \tag{6}$$

where $E_e(E'_e)$ is the incident (scattered) electron energy and θ_e is the scattered electron angle. The extension of the kinematic range was performed by taking a set of data with the interaction vertex shifted in such a way that smaller θ_e could be probed, and by using initial state radiation events where E_e is reduced. The preliminary data at low Q^2 for the ZEUS [64] and H1 [65] experiments are shown in Fig. 12. There is good agreement between the two measurements. The rise of F_2 with decreasing x is

seen to persist down to these low Q^2 values, although the slope is decreasing. The data are compared to several parton density parametrizations. The DL prediction is ruled out for Q^2 values above 2 GeV^2 and is disfavored at $Q^2 = 1.5$ GeV^2. The GRV predictions are seen to agree well with the data over the full range of measurements. The agreement between E665 data and GRV at higher values of x is seen to persist down to the smaller x ($x \geq 2 \cdot 10^{-5}$) measured at HERA. The success of these perturbative QCD calculations at such a low scale is somewhat unexpected, despite the predictions of the GRV group. The data are also compared to the MRS and CTEQ parametrizations. These parametrizations are in reasonable agreement with the data.

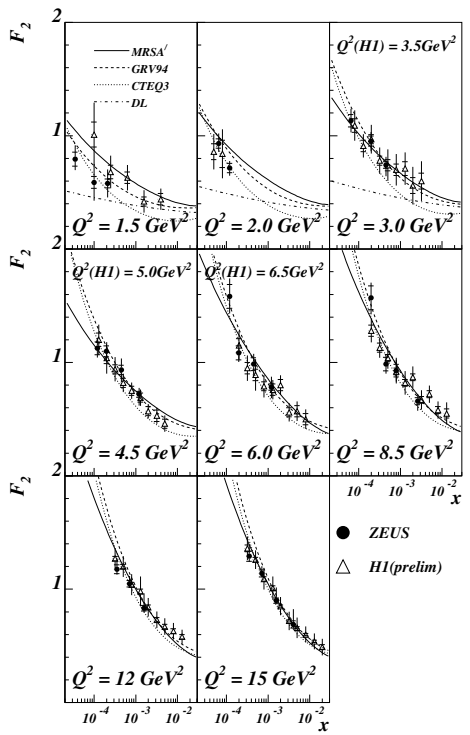

Fig. 12. Recent results from ZEUS and H1 on F_2 at low Q^2. Note that in some bins the H1 and ZEUS data are at different Q^2.

6.2. Double Asymptotic Scaling

The success of the GRV approach implies that the DGLAP equations are capable of describing the data down to very low values of Q^2 (≈ 0.5 GeV^2 in the E665 case.) It is therefore of interest to compare other predictions of this formalism to the data. One such prediction goes by the name double asymptotic scaling [61] (see the report of Jochen Bartels for a detailed descritpion). The DGLAP evolution equations are

rewritten in terms of the variables

$$\sigma = \sqrt{\ln(\frac{x_0}{x})\ln(\frac{t}{t_0})}$$
$$\rho = \sqrt{\frac{\ln(\frac{x_0}{x})}{\ln(\frac{t}{t_0})}}$$

where $t \equiv \ln Q^2/\Lambda^2$. The measured values of F_2 are rescaled by functions $R_F(\sigma,\rho)$ and $R'_F(\sigma,\rho)$ to remove the part of the leading subasymptotic behavior which can be calculated in a model independent way. The results for the preliminary H1 [65] F_2 measurements are shown in Fig. 13. Scaling is found to set in for $\rho \geq 1.5$. Note that Q_0 represents here the value at which F_2 is flat. In a previous analysis [63], H1 found that a value of $Q_0^2 = 1$ GeV^2 could be used to represent the data. These new measurement however require a lower value of $Q_0 = 0.5$ GeV^2. Although the physical meaning of these scaling variables is not clear, the results can be interpreted to indicate that the DGLAP formalism is valid down to very low values of Q^2.

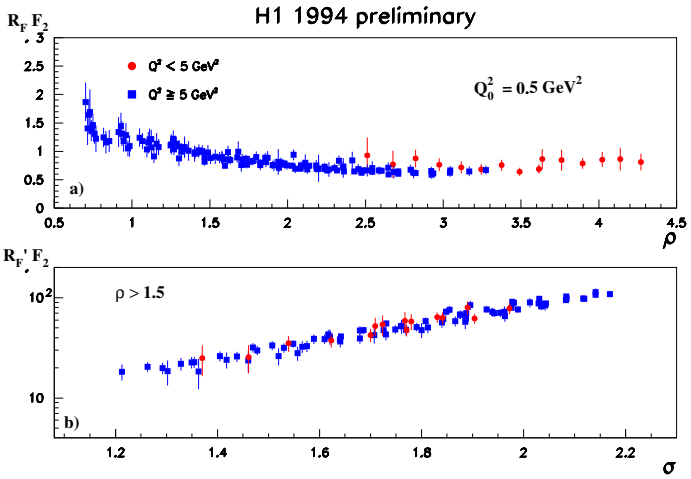

Fig. 13. Scaling of the structure functions versus ρ and σ.

6.3. Summary of F_2 Measurements

A summary of the fixed target measurements and HERA results is shown in Fig. 14. The results are plotted versus Q^2 at fixed x. These beautiful data show a smooth transition from the fixed target data to the HERA data. Over three orders of magnitude are measured in Q^2 at fixed x (and vice versa). The observed scaling violations are in good agreement with the predictions of perturbative QCD.

6.4. Total Virtual Photon—Proton Cross Section

The differential cross section for electron-proton scattering given in equation 3

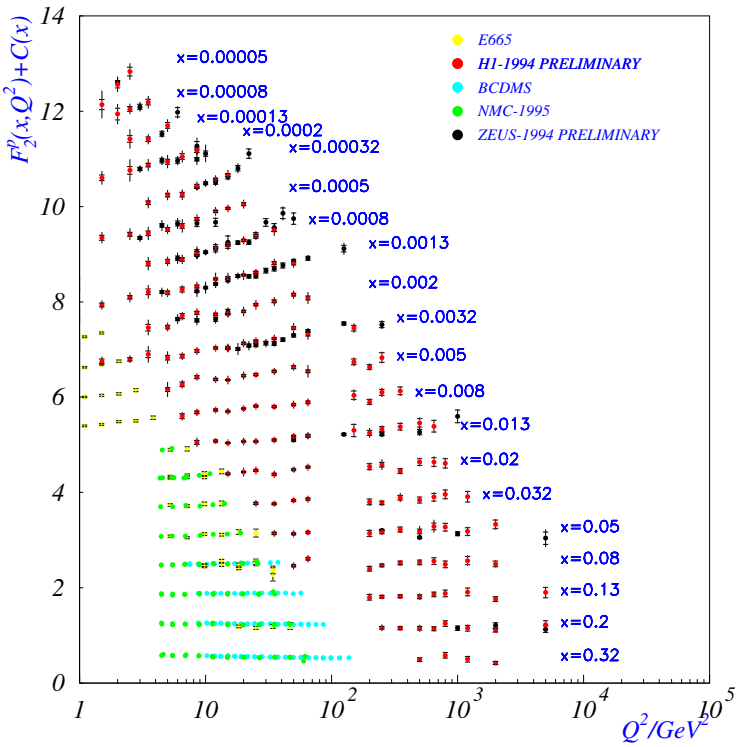

Fig. 14. Summary of fixed target and HERA data on F_2^p. The data are plotted vs. Q^2 for fixed x.

can be rewritten as follows:

$$\frac{d^2\sigma}{dxdQ^2} = \Gamma\sigma_{Tot}^{\gamma^* p} \tag{7}$$

where Γ represents the flux of virtual photons and $\sigma_{Tot}^{\gamma^* p} = \sigma_T + \epsilon\sigma_L$ is the total virtual photon—proton cross section. Here ϵ is the relative longitudial polarization of the virtual photon. At small–x, the relationship

$$F_2(x,Q^2) \approx \frac{Q^2}{4\pi^2\alpha}\sigma_{Tot}^{\gamma^* p} \tag{8}$$

holds, such that F_2 and $\sigma_{Tot}^{\gamma^* p}$ have the same x (or W) dependence. The virtual photon-proton cross section is shown as a function W in Fig. 15. The HERA data indicate a steep rise in the cross section down to $Q^2 = 2.0$ GeV^2. Below this value of Q^2, the only HERA data is for photoproduction ($Q^2 \approx 0$ GeV^2). The total photoproduction cross section, also shown in Fig. 15, has a W dependence consistent with that found in hadron-hadron scattering. The value of Q^2 at which these two different behaviors merge is unknown, and is one of the interesting experimental questions to be answered at HERA. The nature of this transition is clearly an important theoretical topic. An extended discussion can be found in the report of C. Berger in these proceedings.

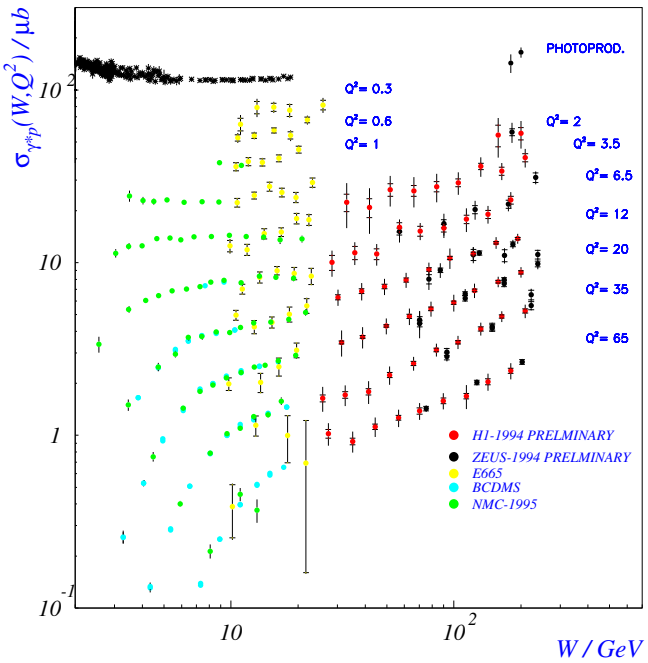

Fig. 15. W dependence of $\sigma_{Tot}^{\gamma^* p}$ from recent HERA data. Also shown are results from fixed target experiments and the total photoproduction cross section.

6.5. The Gluons in the Proton - Inclusive Method

The standard method for extracting the gluon density in the proton is based on the logarithmic derivative of F_2:

$$\frac{dF_2(x,Q^2)}{d\ln Q^2} = \frac{\alpha_S(Q^2)}{2\pi}\left[\int_x^1 \frac{dz}{z}\frac{x}{z}P_{qq}(x/z)F_2(z,Q^2) + 2\sum_q e_q^2 \int_x^1 \frac{dz}{z}\frac{x}{z}P_{qg}(x/z)zg(z,Q^2)\right] \tag{9}$$

where the sum runs over quark flavors. P_{qq} and P_{qg} are the quark splitting functions to two quarks and to a quark plus gluon, respectively. The gluon density is represented by g. The splitting functions can be calculated (perturbatively), and as a result the Q^2 dependence of the parton densities may be calculated provided their x dependence is known at some Q^2. A very common approach is to parameterize at fixed $Q^2 = Q_0^2$ the x dependence of the parton densities by

$$x \cdot \text{density}(x,Q_0^2) = Ax^{-\delta}(1-x)^{\eta} \cdot \text{polynomial}(\sqrt{x}), \tag{10}$$

or some other similar form, giving each parton density its own set of parameters. The parameters are then determined by using the evolution equations to perform a fit to F_2 over a wide range of x and Q^2.

This approach has been used in fixed target experiments [66] as well as by ZEUS [62] and H1 [63]. The HERA results are shown in Fig. 16. The results from approximate methods (Prytz [67], EKL [68]) are found to be in good agreement with the DGLAP fit. The values from the NMC collaboration are also shown, and agree within the range of uncertainty of the measurements. ZEUS finds $0.25 < \delta < 0.39$ at $Q_0^2 = 7$ GeV^2, while H1 finds $\delta = 0.22$ at $Q_0^2 = 4$ GeV^2, reflecting the rise of F_2 for decreasing x. As can be seen in the figure, the extracted gluon densities are in good agreement.

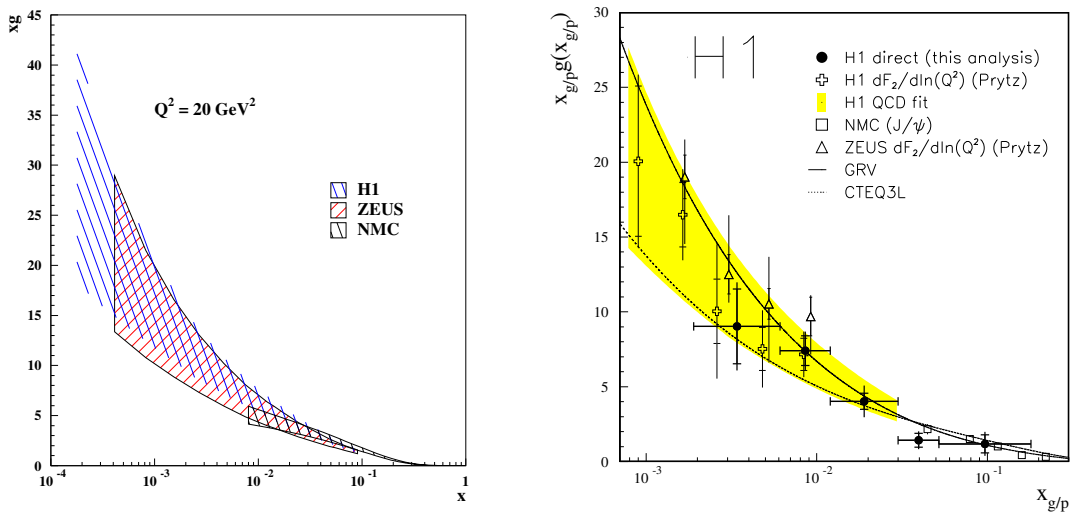

Fig. 16. The gluon momentum density in NLO from ZEUS, H1, and NMC at $Q^2 = 20$ GeV^2 are shown in the left plot. The errors on the fits are given by the shaded region. The measurement of the gluon momentum density in the proton in LO from photon-gluon fusion into 2 jets by the H1 collaboration is shown in the right plot (at a scale of $Q^2 = 30$ GeV^2). The result from the NMC collaboration using photon-gluon fusion into J/ψ is also shown, along with the LO F_2 fit result from H1 and the result of approximate methods from H1 and ZEUS.

6.6. Gluon Density Extraction from Direct Methods

In addition to these fits to F_2, the gluon density can be extracted using other techniques. For instance, the NMC collaboration has measured the gluon momentum density using inelastic J/ψ production via photon–gluon fusion [69]. This process is shown schematically in Fig. 17. In this process, the scale at which the gluon density is probed is expected to depend on the mass of the J/ψ.

The H1 collaboration has also used photon-gluon fusion events, but in this case for jet production [70]. In LO, two jet events in DIS are produced either by photon-gluon fusion, or by QCD-Compton scattering where a hard gluon is radiated from a quark. At small–x, the cross section is expected to be dominated by photon-gluon fusion. These LO extractions of the gluon momentum density are compared in Fig. 16 to the ZEUS and H1 results from fits to F_2. These different methods are found to be in good agreement. This consistency provides a nontrivial check for the universality of

the gluon density.

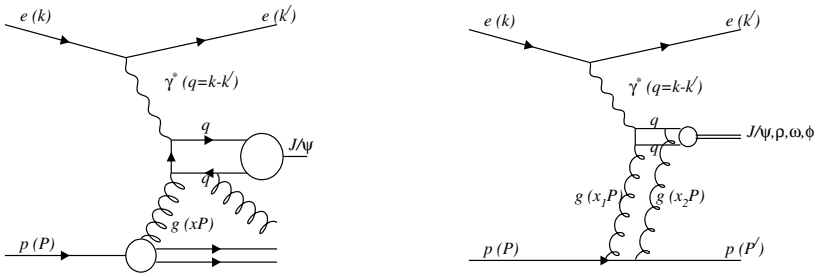

Fig. 17. The production of vector mesons via one and two gluon exchange.

There are other methods which have been proposed for the measurement of the gluon density, such as exclusive vector meson production [71] and diffractive jet production [72]. These methods are quite promising since they depend on the square of the gluon momentum density. They are however all LO calculations, where the scales at which the gluon density is probed is not well defined. The x value at which the gluon density is probed is under some discussion, and is probably not known to better than a factor of 2. There is also in some cases an unknown two-gluon correlation factor which enters the calculation. While these methods are quite promising, there clearly remains some theoretical work to be done before they can be considered on the same level as the fits to F_2. In particular, higher order corrections need to be estimated.

7. Recent Results from the Tevatron

The structure of the proton can be probed at $p\overline{p}$ colliders in a way similar to the probing of the photon at HERA; i.e., the structure is probed using quarks and gluons. A hard scale is set by requiring jet production. Cross sections and angular distributions can then be compared to MC simulations using different input parton densities to see which give the best representation of the data.

7.1. W Production Asymmetry

CDF [73] has studied the decay angular distributions of $W^{\pm}$ to constrain the ratio of parton densities $\frac{d(x)}{u(x)}$. In $p\overline{p}$ collisions, the W^+ is preferentially produced in the direction of the proton since $u(x)$ is peaked at higher values of x than $d(x)$. Conversely, W^- is produced preferentially in the direction of the $\overline{p}$. Experimentally, one studies the angular distribution of the decay lepton, which folds in the $V-A$ decay angular distribution for the W. The shape of the resulting angular distribution after event selection cuts is sensitive to the ratio $\frac{d(x)}{u(x)}$ in the x range $0.007 < x < 0.27$. The

92-93 CDF data [73] from this type of analysis have been used by the CTEQ, MRS and GRV groups to constrain their parton distributions. Recent results from the CDF collaboration [74] from their 1994 data run are shown in Fig. 18. In this plot, the charge asymmetry

$$A(y_l) = \frac{dN_+(y_l)/dy_l - dN_-(y_l)/dy_l}{dN_+(y_l)/dy_l + dN_-(y_l)/dy_l} \,, \tag{11}$$

where $N_\pm$ is the observed number of positively(negatively) charged leptons, is plotted versus y_l (the lepton pseudorapidity). These new data are compatible with the previous data as well as with the latest parton distributions.

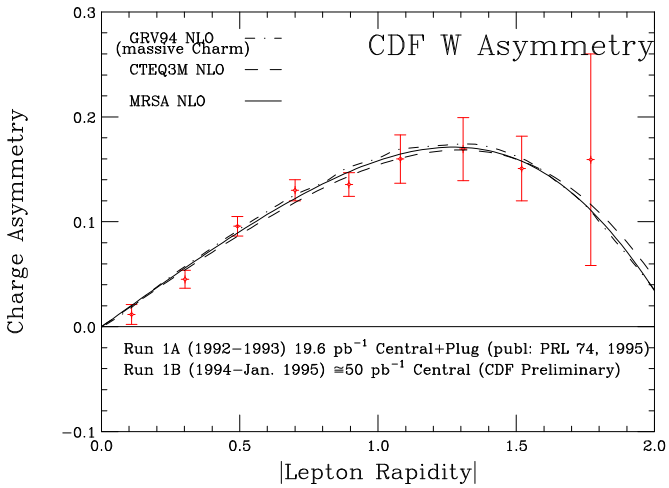

Fig. 18. The W asymmetry from CDF. The mean charge asymmetry (see text) is plotted as a function of the rapidity of the detected lepton.

7.2. Dijet Cross Section

D0 has probed the parton density in the proton via the angular distribution for dijets [75]. When both jets are in the same hemisphere of the detector, the kinematics corresponds to the scattering of one large–x parton and one small–x parton. When the jets are back to back, the jets have roughly the same x. In this case, forward jets correspond to larger values of x. Typical x values for centrally produced jets are $x \approx 0.05$. The triply differential cross section (as a function of the two jet rapidities and E_T) was measured. The quantity $\eta_2 \cdot \mathrm{Sign}(\eta_1)$ is then defined. This quantity is positive when the jets are in the same hemisphere, and negative when the jets are in opposite hemispheres. The results for $< d\sigma/d\eta_2 \cdot \mathrm{Sign}(\eta_1) > \mathrm{E_T}\eta_1$ are plotted in Fig. 19, compared with a prediction using the CTEQ2M (NLO) parton distribution set. The uncertainty arising from the energy scale is shown by the dashed lines. D0 concludes that existing parton distributions have too many gluons for $x > 0.1$, and that no parton distribution sets work for the full range measured. However, the large

systematic error from the energy scale needs to be reduced to make this a stronger test.

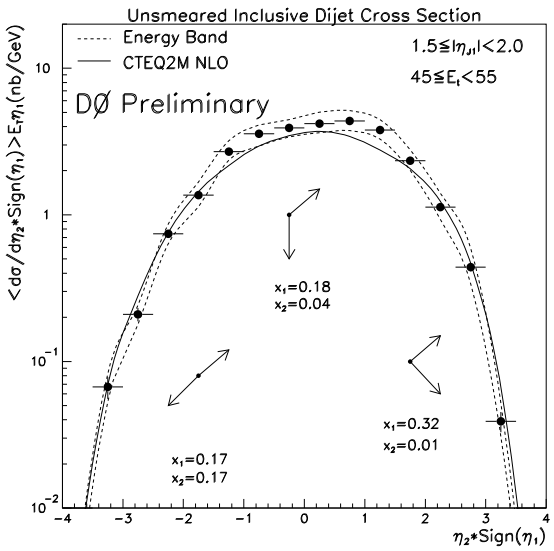

Fig. 19. The inclusive dijet cross section, $d^3\sigma/dE_T d\eta_1 d\eta_2$ as a function of $\eta_2 \cdot Sign(\eta_1)$ from D0. The diagrams indicate the topology and approximate x values being probed in the different regions.

7.3. Prompt Photon Production

Prompt photon production, where a high p_T photon is radiated from the scattered quark (or incoming quark) is a sensitive probe to the gluon density in the proton. In LO, the scattering is simply $q + g \rightarrow q + \gamma$. The D0 collaboration [76] has measured the inclusive cross section for photons in the central rapidity region as a function of p_T. This spectrum is compared to predictions from a NLO QCD calculation [77]. The CTEQ2M parton density set has been used for this comparison and the renormalization scale was chosen at $\mu = p_T$. Good agreement is found between the data and the calculation, contrary to previous results.

The D0 collaboration has also studied the jets recoiling against the photon to test QCD predictions on the angular distributions and to gain further information on the gluon density. These results show good agreement with the NLO QCD calculations.

8. High Q^2 Cross Sections at HERA

The HERA experiments H1 and ZEUS have measured the differential cross sections $d\sigma/dQ^2$ for both charged and neutral current events, with e^+ and e^- beams. The results are shown in Fig. 20. The cross sections are seen to become equal for $Q^2 \approx M_W^2$ as expected for a massive W propagator. The expected suppression of

charged current events for e^+ is also measured.

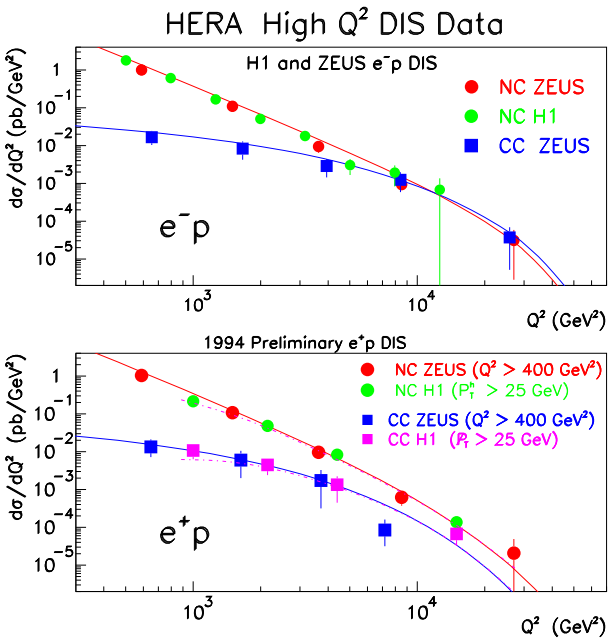

Fig. 20. The neutral and charged current cross sections as a function of Q^2 for the HERA experiments, for electron and positron beams.

9. Outloook and Conclusion

The analysis of fixed target data on the structure of different nuclei is still active, and more results can be expected in the coming years (e.g., F_L from the NMC collaboration). Existing data sets can also be used in imaginative ways to extract interesting physics quantities, as was demonstrated by the CCFR analysis of xF_3 data to measure α_S.

From the collider, the analysis of direct photon events should provide powerful constraints on the gluon density in the proton. Also, Drell-Yan production should give information on the quark distributions.

At HERA, the expansion of the kinematic range continues, with new results expected at higher Q^2 from increased luminosity. A full analysis of the different structure functions may also be possible using the polarization option and the ability to run with both e^+ and e^- beams. There is also the possibility of running with deuterons. At the lower Q^2 values, new results are expected due to improvements in the detectors. Measurements should become available down to $Q^2 = 0.2$ GeV^2 by next year. Systematic errors are expected to keep improving, and there is a real possibility for an F_L measurement at HERA soon.

There is a currently a sense of excitement in the community of physicists study-

ing the photon and proton structure. This has come about from the quantity and quality of new data which has become available in recent years, and from the intense theoretical activity accompanying it. There is the expectation that qualitatively new knowledge will results from this tremendous activity. I hope I have transmitted some of this in my presentation.

10. Acknowledgements

I would like to thank Albert DeRoeck, John Parsons and in particular Aharon Levy for a careful reading of the manuscript. I would also like to thank Jon Butterworth for useful discussions.

1. J. C. Collins, D. E. Soper and G. Sterman, in *Perturbative Quantum Chromodynamics, Advanced Series on Directions in High Energy physics, Vol 5* ed. A. H. Mueller, (World Scientific 1989).
2. DELPHI Collab., paper submitted to *EPS-HEP 95* **Ref. eps0573**.
3. L3 Collab., paper submitted to *EPS-HEP 95* **Ref. eps0096**.
4. E. Witten, *Nucl. Phys.* **B 120** (1977) 189.
5. H. Kolanoski, *Two–Photon Physics at e^+e^- Storage Rings* (Springer–Verlag, Berlin, 1984).
6. M. Drees and R. M. Godbole, *Resolved Photon Processes*, preprint **MADPH-95-898, BU-TH-95/2** July 1995.
7. T. Uematsu and T. F. Walsh, *Nucl. Phys.* **B199** (1982) 93.
8. OPAL Collab., paper submitted to *EPS-HEP 95* **Ref. eps0341**.
9. AMY Collab., S. K. Sahu et al., *Phys. Lett.* **B 346** (1995) 208.
10. J. H. Field, F. Kapusta and L. Poggioli *Phys. Lett.* **B 181** (1986) 362; J. H. Field, F. Kapusta and L. Poggioli *Z. Phys. C.* **36** (1987) 121; F. Kapusta, *Z. Phys. C.* **42** (1989) 225.
11. TOPAZ collab., K. Muramatsu et al., *Phys. Lett.* **B 332** (1994) 477.
12. M. Glück, E. Reya and A. Vogt, *Phys. Rev.* **D 45** (1992) 3986.
13. L. E. Gordon and J. K. Storrow, *Z. Phys.* **C 56** (1992) 307.
14. H. Abramowicz, K. Charchula and A. Levy, *Phys. Lett.* **B 269** (1991) 458.
15. D. W. Duke and J. F. Owens, *Phys. Rev.* **D 26** (1982) 1600.
16. T. F. Walsh *Phys. Lett.* **B 101** (1981) 263; F. Borzumati and G. Schuler *Z. Phys.* **C 58** (1993) 139; M. Drees and R. M. Godbole *Phys. Rev.* **D50** (1994) 3124.
17. H1 Collab., I. Abt et al., *Phys. Lett.* **B 314** (1993) 436.
18. ZEUS Collab., M. Derrick et al., *Phys. Lett.* **B 342** (1995) 417.
19. P. Aurenche et al., *Phys. Lett.* **B 338** (1994) 98.
20. M. Klasen, G. Kramer, and S. G. Salesch, DESY preprint **DESY 94-232**.
21. M. Klasen, G. Kramer, DESY preprint **DESY 95-159**.
22. ZEUS Collab., M. Derrick et al., *Phys. Lett.* **B 348** (1995) 665.
23. H1 Collab., paper submitted to *EPS-HEP 95* **Ref. eps0476**.

24. T. Sjöstrand and M. van Zijl, *Phys. Rev* **D 36** (1987) 2019; G. A. Schüler and T. Sjöstrand, *Nucl. Phys.* **B 407** (1993) 539; J. M. Butterworth and J. R. Forshaw, *J. Phys.* **G 19** (1993) 1667; J. M. Butterworth and J. R. Forshaw, in *Proceedings of the Workshop on Two–Photon Physics at LEP and HERA* ed. G. Jarlskog and L. Jönsson, LUND, May 26-28, 1994.
25. A. Capella et al., *Phys. Rep.* **236** (1994) 227.
26. T. Sjöstrand, preprint CERN-TH-6488 (1992); T. Sjöstrand *Comput. Phys. Commun.* **82** (1994) 74.
27. M. Glück, E. Reya and A. Vogt, *Phys. Rev.* **D 46** (1992) 1973.
28. M. Glück, E. Reya and A. Vogt *Z. Phys.* **C 53** (1992) 127; M. Glück, E. Reya and A. Vogt *Phys. Lett.* **B 306** (1993) 391; M. Glück, E. Reya and A. Vogt *Z. Phys.* **C 67** (1995) 433.
29. AFS Collab., T. Akesson et al., *Z. Phys.* **C 34** (1987) 163; UA2 Collab., J. Alitti et al., *Phys. Lett.* **B 268** (1991) 145; CDF Collab., L. J. Keeble et al., *A study of four jet events and search for double parton scattering at* $\sqrt{s} = 1.8$ *TeV*, preprint **FERMILAB-CONF-92-161-E** (1992).
30. H1 Collab., T. Ahmed et al., *Nucl. Phys.* **B 445** (1995) 195.
31. ZEUS Collab., paper submitted to *EPS-HEP 95* **Ref. eps0380**.
32. ZEUS Collab., M. Derrick et al., *Phys. Lett.* **B 349** (1995) 225.
33. H1 Collab., paper submitted to *EPS-HEP 95* **Ref. eps0457**.
34. S. Frixione et al., *Phys. Lett* **B 348** (1995) 633; preprint **CERN-TH/95-143**.
35. A. D. Martin, R. G. Roberts and W. J. Stirling, preprint **RAL-94-055** (1994).
36. M. Drees and R. M. Godbole, preprint **LNF-95/020** (1995).
37. V. N. Gribov and L. N. Lipatov, *Sov. J. Nucl. Phys.* **15** (1972) 1; L. N. Lipatov, *Sov. J. Nucl. Phys.* **20** (1975) 94; G. Altarelli and G. Parisi, *Nucl. Phys.* **B 126** (1977) 298; Yu. L. Dokshitzer, *Sov. Phys. JETP* **46** (1977) 641.
38. E. A. Kuraev, L. N. Lipatov and V. S. Fadin, *Sov. Phys.* **JETP 45** (1977) 199; Ya. Ya. Balitsky and L. N. Lipatov, *Sov. J. Nucl. Phys.* **28** (1978) 822.
39. L. V. Gribov, E. M. Levin and M. G. Ryskin, *Phys. Rep.* **100** (1983) 1; A. H. Mueller and N. Quiu, *Nucl. Phys.* **B 268** (1986) 427.
40. A. Donnachie and P. V. Landshoff *Z. Phys.* **C 61** (1994) 139.
41. A. D. Martin, R. G. Roberts and W. J. Stirling, *Phys. Rev* **D 50** (1994) 6734; A. D. Martin, R. G. Roberts and W. J. Stirling, *Phys. Rev* **D 51** (1994) 4756.
42. H.L. Lai et al, Global QCD Analysis and the CTEQ parton distributions, **CTEQ-404, HEP-PH-9410404** (1994).
43. NMC collab., M. Arneodo et al., preprint **CERN-PPE/95-138** (1995), submitted to *Phys. Lett.*
44. NMC collab., P. Amaudruz et al., *Phys. Lett.* **B 295** (1992) 159.
45. L. W. Whitlow et al., *Phys. Lett.* **B 282** (1992) 475.
46. BCDMS collab., A. C. Benvenuti et al., *Phys. Lett.* **B 233** (1989) 485; BCDMS collab., A. C. Benvenuti et al., *Phys. Lett.* **B 237** (1990) 592.

47. A. Milsztajn et al., *Z. Phys.* **C 49** (1991) 527.
48. A.V. Kotwal et al., XXXth Rencontres de Moriond, March 1995, preprint **Fermilab Conf-95/046-expt** (1995).
49. ZEUS collab., M. Derrick et al., *Z. Phys.* **C 65** (1995) 379.
50. H1 collab., T. Ahmed et al., *Nucl. Phys.* **B 439** (1995) 471.
51. B. Badelek and J. Kwiecinski, *Phys. Lett.* **B 295** (1992) 263.
52. J. Conrad et al., in *Proceedings of 15TH Workshop on Weak Interactions and Neutrinos (WIN 95)*, 4-8 Sep 1995 , Talloires, France.
53. D. J. Gross and C. H. Llewellyn Smith, *Nucl. Phys* **B 14** (1969) 337.
54. CCFR collab., paper submitted to *EPS-HEP 95* **Ref. eps043**.
55. S. A. Larin and J. A. M. Vermarseren, *Phys. Lett.* **B 259** (1991) 345.
56. V. M. Braun and A. V. Kolesnichenko, *Nucl. Phys.* **B 283** (1987) 723.
57. P. C. Bosetti et al., *Nucl. Phys.* **B142** (1978) 1; Ammosov et al., *JETP* **36** (1982) 300; Allasia et al., *Z. Phys* **C 28** (1985) 321; Ammosov et al., *Z. Phys* **C 30** (1986) 175; Varvell et al., *Z. Phys.* **C 36** (1987) 1.
58. W. J. Marciano, *Phys. Rev.* **D 29** (1984) 580.
59. ZEUS collab., M. Derrick et al., *Phys. Lett.* **B 316** (1993) 412.
60. H1 collab., I. Abt et al., *Nucl. Phys.* **B 407** (1993) 515.
61. R. D. Ball and S. Forte, *Phys. Lett.* **B 335** (1994) 77; R. D. Ball and S. Forte, *Phys. Lett.* **B 336** (1994) 77.
62. ZEUS collab., M. Derrick et al., *Phys. Lett.* **B 345** (1995) 399.
63. H1 collab., S. Aid et al., *Phys. Lett.* **B 354** (1995) 494.
64. ZEUS collab., M. Derrick et al., submitted to *Z. Phys.*, preprint DESY 95-193.
65. H1 Collab., paper submitted to *EPS-HEP 95* **Ref. eps0470**.
66. NMC collab., M. Arneodo et al., *Phys. Lett.* **B 309** (1993) 222.; BCDMS collab., A.C. Benvenuti et al., *Phys. Lett.* **B 223** (1989) 490; CDHS collab., P. Berge et al., *Z. Phys.* **C 49** (1991) 187.
67. K. Prytz, *Phys. Lett.* **B 311** (1993) 286; K. Prytz, *Phys. Lett.* **B 332** (1994) 393.
68. R. K. Ellis, Z. Kunszt and E. M. Levin, *Nucl. Phys.* **B 420** (1994) 517, and Erratum in *Nucl. Phys.* **B 433** (1995) 498.
69. NMC collab., D. Allasia et al., *Phys. Lett.* **B 258** (1991) 493.
70. H1 collab., S. Aid et al., *Nucl.Phys.* **B 449** (1995) 3.
71. M. G. Ryskin,*Z. Phys.* **C 57** (1993) 89; S. J. Brodsky et al.,*Phys. Rev.* **D 50** (1994) 3134; B. Z. Kopeliovich et al.,*Phys. Lett.* **B 324** (1994) 469.
72. N. N. Nikolaev and B. G. Zakharov,*Phys. Lett.* **B 332** (1994) 177.
73. F. Abe et al., *Phys. Rev. Lett.* **74** (1995) 850.
74. CDF collab., paper submitted to *EPS-HEP 95* **Ref. eps025**.
75. D0 collab., presented by Freedy Nang,*Tenth Topical Workshop on Proton-Antiproton Collider Physics*, Fermilab, May 1995.
76. D0 Collab., paper submitted to *EPS-HEP 95* **Ref. eps0498**.
77. B. Bailey, J. F. Owens, and J. Ohnemus, *Phys. Rev.* **D 46** (1992) 2018.